Spatiotemporal dynamics in the coherence collapsed regime of semiconductor lasers with optical feedback

Cristina Masoller
Instituto de Física, Facultad de Ciencias, Universidad de la República, Montevideo, Uruguay

(Received 2 January 1997; accepted for publication 9 June 1997)

This paper presents a spatiotemporal characterization of the dynamics of a single-mode semiconductor laser with optical feedback. I use the two-dimensional representation of a time-delayed system (where the delay time plays the role of a space variable) to represent the time evolution of the output intensity and the phase delay in the external cavity. For low feedback levels the laser output is generally periodic or quasiperiodic and with the 2D representation I obtain quasiperiodic patterns. For higher feedback levels the coherence collapsed regime arises, and in the 2D patterns the quasiperiodic structures break and ''defects'' appear. In this regime the patterns present features that resemble those of an extended spatiotemporally chaotic system. The 2D representation allows the recognition of two distinct types of transition to coherence collapse. As the feedback intensity grows the number of defects increases and the patterns become increasingly chaotic. As the delay time increases the number of defects in the patterns do not increase and there is a signature of the previous quasiperiodic structure that remains. The nature of the two transitions is understood by examining the behavior of various chaotic indicators (the field autocorrelation function, the Lyapunov spectrum, the fractal dimension, and the metric entropy) when the feedback intensity and the delay time vary. © *1997 American Institute of Physics.*
[S1054-1500(97)00903-8]

Single-mode semiconductor lasers are often used in optical communication systems because they are compact, relatively inexpensive, and can be modulated at high speeds. However, unwanted reflections (even of the order of 1% of the emitted power) from an optical disk or optical fiber frequently destabilize the laser and induce a transition to a chaotic state, which has been called coherence collapsed state, and is characterized by a broadband spectrum (the linewidth increases from a few megahertz to several gigahertz). The phenomenon is important both for its theoretical interest and practical applications. In this paper I study the dynamics in the chaotic regime, and effects of varying the intensity of the light fed back into the laser cavity, and the distance of the external reflector. I use the two-dimensional representation of time-delayed systems to represent the time evolution of the laser variables as 2D patterns. When the delay time is much longer than the intrinsic oscillation period, there are two very different time scales in the dynamics. In addition, there are time-localized events, which correspond to jumps among coexisting chaotic attractor ruins. This leads to chaotic patterns that resemble those arising from extended spatiotemporally chaotic systems. I show that 2D representation provides a powerful tool for the visualization of some features of the dynamics, hidden in the time evolution of the variables. When the feedback intensity increases, the dynamics become more chaotic, and the patterns appear increasingly irregular. On the contrary, when the distance of the external reflector increases, although the dimension of the attractor grows, the patterns do not appear increasingly disorganized. I explain these results by examining the behavior of various chaotic indicators.

I. INTRODUCTION

In recent years semiconductor lasers have been extensively used in optical communication systems because they are compact and efficient and can be modulated directly at relatively high speeds. Unfortunately, they are particularly sensitive to reflections from a surface of another device such as an optical disk or optical fiber.[1]

It is well known that a dynamical system can be either stabilized or destabilized by a feedback loop. Laser diodes are good examples of this rule. Optical feedback can be used for mode stabilization and spectral linewidth narrowing,[2] but one must carefully choose the external cavity parameters, because optical feedback can also induce the transition to the coherence collapsed regime.[3] In this regime the laser linewidth broadens from a few megahertz to several gigahertz and the dynamics is chaotic.[4]

The governing equations of a single-mode semiconductor laser with weak and moderate optical feedback are the Lang and Kobayashi[5] rate equations. They are the standard laser equations plus a time-delayed term that accounts for the field reflected from the external mirror (for low feedback levels multiple reflections can be neglected). The external

cavity is described by two parameters: the feedback parameter, γ, which is proportional to the strength of the feedback, and the delay time, τ, which is proportional to the external cavity length. The model gives a good understanding of the observed laser behavior, such as the linewidth reduction for low feedback levels and the transition to the coherence collapsed regime for higher feedback.[6,7]

A single-mode laser coupled to an external cavity is a multimode laser because the external cavity adds a series of new modes, which are the so-called external cavity modes (ECMs). The ECMs are the fixed point solutions of the Lang and Kobayashi equations. They are created in pairs after saddle-node bifurcations and their number grows with the value of $C=\gamma\tau\sqrt{1+\alpha^2}$ (Ref. 4) (where α is the linewidth enhancement factor[8,9]). For increasing feedback (or increasing delay time) the initially stable external cavity modes become unstable due to Hopf bifurcations, and quasiperiodic routes to chaos occur as the feedback parameter (or the delay time) is increased further.[4] If C is large enough, several coexisting chaotic attractors can be found.[10] Stronger feedback destabilizes all the coexisting attractors and induces the coherence collapsed regime. In this regime a global attractor forms from the ruins of the single ECM attractors, and the laser switches among all the merged attractor ruins.

In Ref. 11 I analyzed the dynamics of the Lang and Kobayashi model when the delay time is short (a few relaxation oscillation periods of the solitary laser) and the feedback level is below the onset of attractor merging. In this case the ECM attractors are generally low dimensional (fixed points, limit cycles, and two-torus). Regions of improved stability exist for values of τ such that $\tau/\tau_R \approx n$ (where τ_R is the period of the relaxation oscillations of the solitary laser, and n is an integer number). In these resonances the attractor reverses the route to chaos: if it was a limit cycle, in the resonance it becomes a fixed point; or if it was a two-torus, in the resonance it becomes a limit cycle. As the delay time increases the width of the resonant regions decreases and they become more difficult to detect.

In this paper I proceed further and study the high dimensional dynamics that is induced by moderately strong optical feedback (above the onset of attractor merging) from a large external cavity (τ much larger than the relaxation oscillation period).

Farmer[12] was the first to investigate in detail the properties of a delay dynamical system in the long delay limit. Farmer studied the Mackey–Glass model, which describes the creation of blood cells, and found that as the delay time is increased the Lyapunov spectrum, λ_i, decreases as $1/\tau$, the metric entropy, h_μ, remains roughly constant, and the Lyapunov dimension, D, grows linearly. Similar results were found by Ikeda and Matsumoto[13] in the Ikeda model of a nonlinear optical resonator and by Le Berre *et al.*[14] in a nonlinear ring cavity. In these models the nonlinear interactions pertain only to the delayed term. Lepri *et al.*[15] studied a more general class of iterative delay maps, which includes a local nonlinear coupling, and found that the local nonlinear interaction was responsible for the existence, under certain conditions, of an anomalous component of the Lyapunov spectrum (λ_1) which does not scale as $1/\tau$. Nevertheless, it was found that in the long delay time limit the rest of the spectrum scales as $1/\tau$, h_μ remains finite, and D grows linearly. Therefore, it can be conjectured that the asymptotic behavior of the dimension and entropy with τ are generic properties of time-delayed systems, while the behavior of the Lyapunov spectrum depends on the nonlinearity of the equations.

The scaling properties of the chaotic indicators of a delay dynamical system in the $\tau\to\infty$ limit have analogies with those of a one-dimensional (1D) spatially extended system in the $L\to\infty$ limit (where L is the system size).[15] (For example, for 1D spatiotemporal chaotic systems the fractal dimension of the attractor typically grows with L, while for a time delayed system D grows with τ.) This suggests that ideas from extended systems in the $L\to\infty$ limit might be applicable to delayed systems in the $\tau\to\infty$ limit. Arecchi *et al.*[16] introduced a two-dimensional (2D) representation of a time delayed system in the following way: decomposing the continuous time variable, t, into a continuous variable, σ $(0\leqslant\sigma\leqslant\tau)$, and a discrete variable, n

$$t=\sigma+n\tau, \tag{1}$$

a generic time t can be represented by two numbers, n and σ, identifying the delay unit (''time'' variable) and the position inside the delay unit (''spatial'' variable). In this way, a 1D signal arising from a time-delayed system can be rearranged as a 2D pattern of length $L=\tau$.

The 2D representation of a time-delayed system allows a simple visualization of the dynamics, and sheds light on some features of the complex dynamics, hidden in the long 1D series of the data. Giacomelli *et al.*[17] investigated the dynamics of a CO_2 laser with delayed feedback on the losses, and for delays long with respect to the oscillation period found evidence of phase defects and two distinct disordered phases.

In this paper I use the 2D representation to analyze the dynamics of the Lang and Kobayashi model when the optical feedback is from a distant reflector ($\tau\gg\tau_R$).

For feedback levels corresponding to the attractor merging regime, the global attractor that forms from the ruins of the ECM attractors has a large fractal dimension (typically, $D>30$). I am interested in determining whether the dynamics in this regime (which consist of evolution in the ruin of an ECM attractor and jumps among neighboring ruins) has common features with the dynamics usually observed in 1D extended spatiotemporal chaotic systems. Also, I am interested in comparing in this regime the effects of the external cavity parameters. Although both γ and τ increase the number of exited external cavity modes (and induce a quasiperiodic route to chaos in each mode), they have distinct effects when the laser operates in the coherence collapsed regime.

This paper is organized as follows. Section II presents the 2D representation of the dynamics of the laser. The time series of the output intensity and phase delay in the external cavity are arranged as 2D patterns. The dynamics in a single ECM attractor gives rise to quasiperiodic patterns. At the beginning of attractor merging (when few attractors have merged) the quasiperiodic structures break, and ''defects''

appear. I study the effects of varying the feedback intensity and the delay time. As γ increases the number of defects increases, and the previous quasiperiodic structure (corresponding to the evolution in a single ECM attractor) is completely destroyed. As τ increases, defects appear but there is a signature of the previous quasiperiodic structure that remains. These results are explained in Sec. III by examining the behavior of the autocorrelation function of the complex electric field, the Lyapunov spectrum, the fractal dimension, and the metric entropy, when γ and τ vary. Section IV provides a summary and conclusions.

II. TWO-DIMENSIONAL REPRESENTATION OF THE COHERENCE COLLAPSED REGIME

In this section I use the 2D representation introduced by Arecchi *et al.*[16] [Eq. (1)] to recognize spatiotemporal features in the dynamics of the laser in the coherence collapsed regime.

Writing the intracavity complex electric field as $E(t)=E(t)\exp[i(\omega_0 t+\phi(t))]$, where ω_0 is the laser frequency without feedback, the Lang and Kobayashi equations are

$$\frac{d[E(t)e^{i\phi(t)}]}{dt}=\left(\frac{1+i\alpha}{2}\right)\left[G(N,E^2)-\frac{1}{\tau_p}\right]E(t)e^{i\phi(t)} + \gamma E(t-\tau)e^{i\phi(t-\tau)}e^{-i\omega_0\tau}, \tag{2}$$

$$\frac{dN(t)}{dt}=J-\frac{N(t)}{\tau_s}-G(N,E^2)E(t)^2. \tag{3}$$

In these equations $N(t)$ is the carrier population (electron-hole plasma) and the modulus of the electric field $E(t)$ is normalized such that $V_c E(t)^2$ is the total photon number in the laser wave guide (where V_c is the volume of the active region). The external cavity parameters are the feedback parameter, γ, that measures the intensity of the light fed back into the laser cavity, and the delay time, $\tau=2L_{\rm ext}/c$, that is the round-trip time of the light in the external cavity of length $L_{\rm ext}$. Other parameters are: τ_s the carrier lifetime, τ_p the photon lifetime, $G=G_N(N-N_0)(1-\epsilon E^2)$ the gain per unit time, where G_N is the modal gain coefficient, N_0 the carrier density at transparency, and ϵ the nonlinear gain coefficient. α is the linewidth enhancement factor, and J is the current density (in carriers per unit volume and unit time). The quantum noise terms that take into account the effect of spontaneous recombination are omitted since this effect plays a negligible role when the laser is operated well above threshold in coherence collapse.

The simulations were carried out with a fourth-order Runge–Kutta method (with an integration step $\Delta t = 0.01$ ns), and the parameter values given in Table I. In all the simulations the first 500 round-trips in the external cavity are neglected in order to let transients die away. The time sequences of the normalized intensity, $I(t)=E^2(t)/I_{\rm sol}$ (where $I_{\rm sol}$ is the intensity of the solitary laser), and the phase delay in the external cavity, $\Delta\phi(t)=\phi(t)-\phi(t-\tau)$, are represented as 2D patterns.

$\Delta\phi(t)$ is related with the laser mean optical frequency by

TABLE I. Meanings and values of the parameters in Eqs. (2) and (3).

Modal gain coefficient	G_n	8.387×10^{-13} m^3 s^{-1}
Carrier density at transparency	N_0	1.231×10^{24} m^{-3}
Nonlinear gain coefficient	ϵ	2.0×10^{-24} m^3
Photon lifetime	τ_p	1.4 ps
Carrier lifetime	τ_s	1.0 ns
Linewidth enhancement factor	α	4.4
Volume of the active region	V	1.2×10^{-16} m^3
Injected current	$J = 2.0*J_{th}$	4.167×10^{33} m^{-3} s^{-1}
Threshold current	J_{th}	2.083×10^{33} m^{-3} s^{-1}

$$\frac{1}{\tau}\int_t^{t+\tau}\omega(t')dt'=\omega_0+\frac{\Delta\phi}{\tau}. \tag{4}$$

Since the ECMs have optical frequencies ω_i that are separated by approximately 2π, when the laser operates in the ECM attractor developed from mode i, $\Delta\phi$ oscillates around the value $(\omega_i-\omega_0)\tau$, while when the laser operates in coherence collapse, the time evolution of $\Delta\phi(t)$ shows brusque variations (of approximately 2π) that reveal the switching among the merged attractor ruins.

Figure 1 shows the time evolution of $I(t)/I_{\rm sol}$ and $\phi(t)-\phi(t-\tau)$ for increasing γ and $\tau = 10$ ns. For $\gamma = 2.0$ GHz the system evolves in a single ECM attractor. In the time sequences of the intensity and the phase delay [Figs. 1(a), 1(b)], trains of large amplitude oscillations are interrupted by localized events, where the amplitude of the oscillations markedly decreases, and the value of the intensity is approximately constant (equal to the solitary laser value $I_{\rm sol}$). The period of the large amplitude oscillations is approximately the period of the relaxation oscillations of the solitary laser $\tau_R=2\pi\sqrt{\tau_p/G_N I_{\rm sol}}$ ($\tau_R = 0.15$ ns for the parameter values of Table I). The periodicity of the small amplitude oscillations is slightly larger than τ. (The two frequencies that appear in the quasiperiodic route of the external cavity modes are the relaxation oscillation frequency of the solitary laser, $f_{\rm rsol}=1/\tau_R$, and the external cavity frequency, $f_{\rm ext}$, which is slightly lower than $1/\tau$[4].)

For $\gamma\geqslant 2.5$ GHz the ECM attractors begin to merge. The intensity signal [Figs. 1(c), 1(e), 1(g)] appears increasingly chaotic and the plot of $\Delta\phi(t)$ [Figs. 1(d), 1(f), 1(h)] shows that the evolution occurs in several ECM attractor ruins. Note that the rapid variations in the phase delay (originated in the jumps among the attractor ruins) are not reflected in the time evolution of the output intensity.

Figures 2 and 3 show the 2D representation of $I(t)/I_{\rm sol}$ and $\phi(t)-\phi(t-\tau)$ for a fixed delay time ($\tau = 10$ ns) and increasing feedback levels. (In the 1D plots, only 10 delay units were shown, while in the 2D patterns, 1000 delay units are represented.)

When the dynamics occurs in a single attractor, the intensity pattern and the phase delay pattern are very similar, and have the structure of straight lines in a background of thin rolls [Figs. 2(a), 3(a)]. The straight lines represent the regions of small amplitude oscillations, and the thin rolls represent the large amplitude oscillations. This type of pattern appears when the optical feedback is from a large exter-

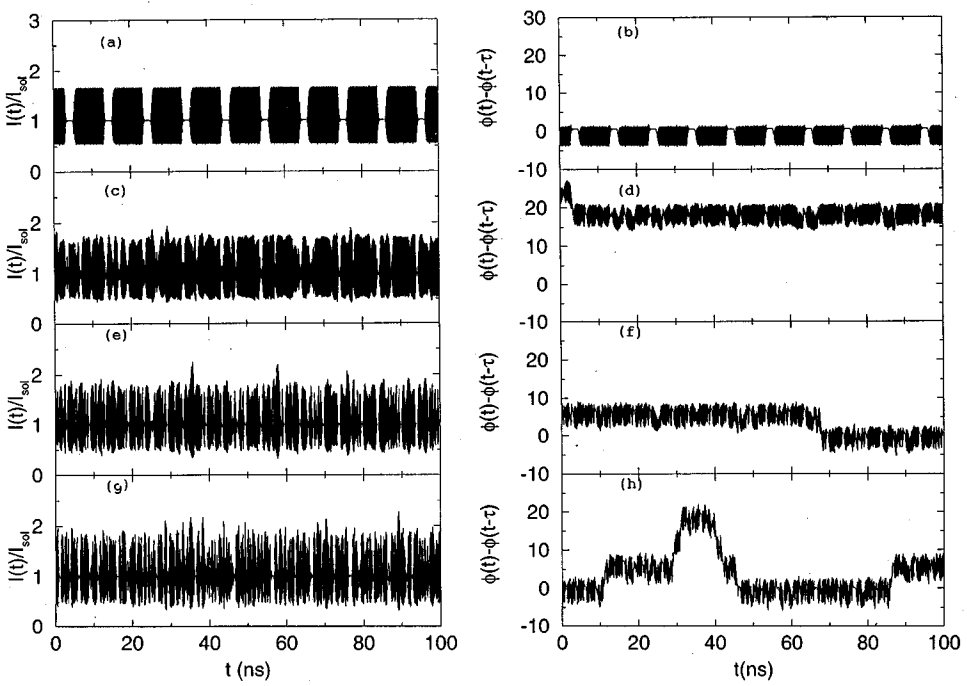

FIG. 1. Time evolution of the output intensity and the phase delay in the external cavity, for $\tau = 10$ ns and (a), (b) $\gamma = 2.0$ GHz; (c), (d) $\gamma = 2.5$ GHz; (e), (f) $\gamma = 3.0$ GHz; (g), (h) $\gamma = 3.5$ GHz.

nal cavity ($\tau \gg \tau_R$) and there are a large number of rolls contained in a single delay unit. The oscillation period τ_R is independent of γ, and therefore the number of the rolls contained in a delay unit is constant for increasing γ (in all the 2D patterns, the spatial length L was set to a value slightly larger than τ, in order to contain an integer number of rolls, and therefore eliminate the drift of the rolls). The straight lines are not vertical but tilted because the periodicity of the regions of small amplitude oscillations is not τ, but slightly larger.

For $\gamma = 2.5$ GHz the ECM attractors begin to merge, and in the intensity pattern [Fig. 2(b)] the dark straight lines break and defects appear. Also, the thin rolls in the background do not form a periodic pattern anymore but present dislocations and asymmetries. The phase delay pattern [Fig. 3(b)] presents in addition a phase structure (three different gray regions) because the evolution occurs in the ruins of three different attractors which have different mean phase delay [in the 1D plot, Fig. 1(d), we observe a brusque jump between two of them].

As γ increases the patterns become increasingly chaotic. In the intensity pattern [Figs. 2(c), 2(d)] the number of defects increase and the straight gray lines are destroyed. Also, the number of phases in the phase delay pattern [Figs. 3(c),

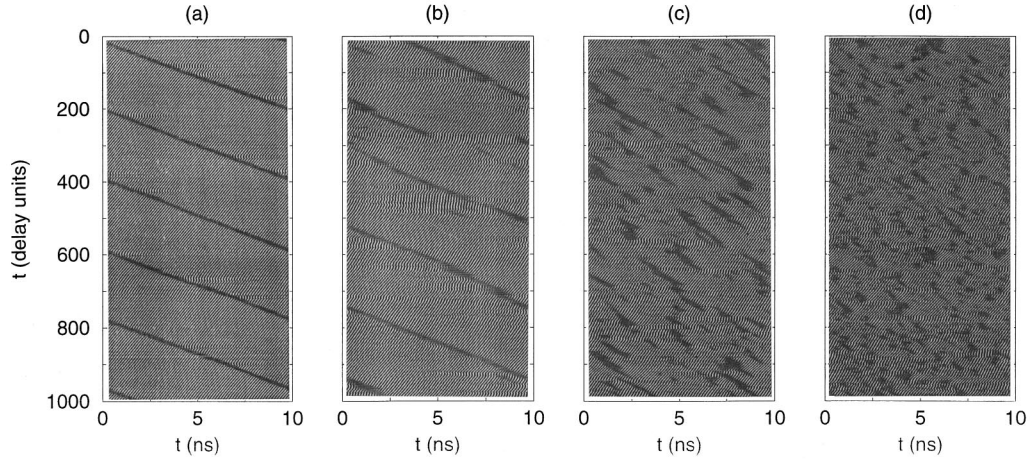

FIG. 2. A 2D representation of the output intensity for $\tau = 10$ ns and (a) $\gamma = 2.4$ GHz; (b) $\gamma = 2.5$ GHz; (c) $\gamma = 3.0$ GHz; (d) $\gamma = 3.5$ GHz. The amplitude of the signals sets the gray scale: the darker (lighter) gray corresponds to the maximum (minimum) data values. 1000 delay units are represented. The horizontal axis ranges over a value slightly larger than τ (there are 504 points sampled with $\Delta t = 0.02$ ns). The ''spatial'' variable increases from left to right, and the ''time'' variable from top to bottom.

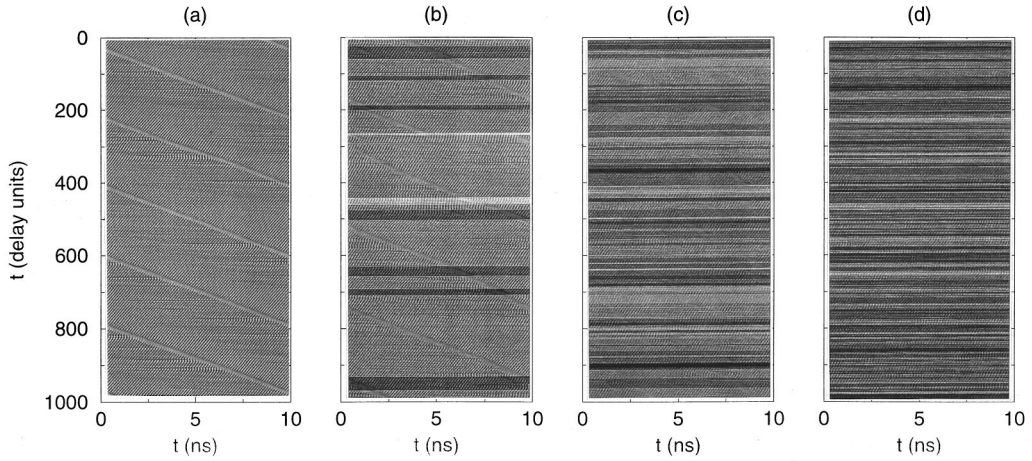

FIG. 3. A 2D representation of the phase delay signal (the same parameters as Fig. 2).

3(d)] rapidly increases and their width decreases, because the number of merged attractors increases and the jumps among them became more frequent.

Figures 4 and 5 show the 2D representations of $I(t)/I_{\mathrm{sol}}$ and $\phi(t)-\phi(t-\tau)$ for a fixed feedback intensity ($\gamma = 2.5$ GHz) and increasing delay time. Since the oscillation period τ_R is independent of τ, the number of rolls contained in a delay unit increases, and therefore in the 2D patterns the rolls appear to become thinner with increasing τ. For $\tau = 5$ ns the dynamics occurs in a single ECM attractor, and the 2D representations of $I(t)/I_{\mathrm{sol}}$ and $\phi(t)-\phi(t-\tau)$ are quasiperiodic patterns [Figs. 4(a), 5(a)]. As τ increases, the ECM attractors merge and defects appear [Figs. 4(b), 4(c), 4(d)]. The gray straight lines are almost horizontal for $\tau = 5$ ns [Fig. 4(a)] and tend to became more vertical as τ increases due to the fact that the periodicity of the small amplitude oscillations is slightly larger than τ, but its difference relative to τ becomes smaller as τ increases.

Contrary to what occurs when γ increases, when τ increases the straight lines are not completely destroyed and the thin rolls in the background remain, forming an almost periodic pattern. Also, in the phase delay pattern [Figs. 5(b), 5(c), 5(d)], there are phases of large width that correspond to attractor ruins where the laser remains a long time before switching to another.

Note that the thin rolls (that represent the large amplitude oscillations) and the straight zones (that represent the small amplitude oscillations) are present in all the phases of the phase delay patterns (see Figs. 3 and 5). The reason is that the frequencies f_{ext} and f_{rsol} are common to all the merged ECM attractors. However, it is interesting that the jumps among the attractor ruins appear to have little or no role in the evolution of the rolls (which evolve in a continuous manner along the pattern). The jumps among the attractor ruins appear to be related only to the apparition of the defects.

Figures 2–5 suggest a transition to a chaotic or highly turbulent regime as γ increases, and to a laminar or weakly turbulent regime as τ increases.

An important advantage of the 2D representation with respect to the 1D time plots or the phase plots of the trajectory, is that in the 2D representation of the phase delay signal we can visualize simultaneously the details of the time evolution in one attractor ruin (i.e., the large amplitude oscilla-

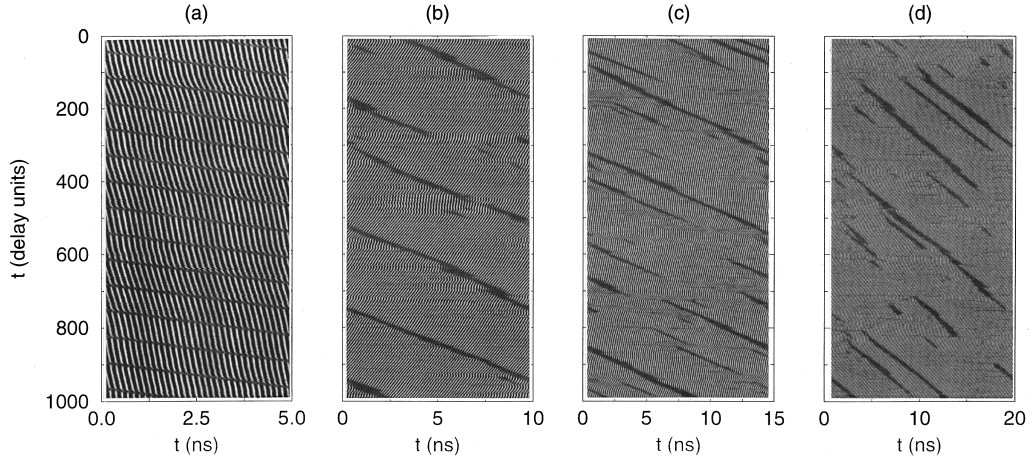

FIG. 4. A 2D representation of the intensity signal, for $\gamma = 2.5$ GHz and (a) $\tau = 5$ ns, (b) $\tau = 10$ ns, (c) $\tau = 15$ ns, and (d) $\tau = 20$ ns.

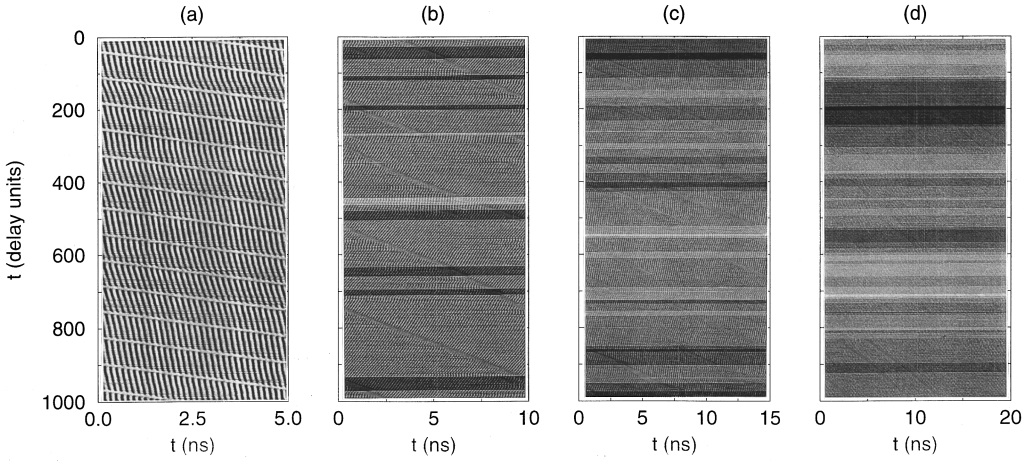

FIG. 5. A 2D representation of the phase delay signal (the same parameters as Fig. 4).

tions, represented by the thin rolls, and the small amplitude oscillations, represented by the defects), and the global features of the dynamics (i.e., the switching among different attractor ruins, represented by the phase structure). The different effects of γ and τ in the dynamics are clearly distinguished in the 2D representation, while they are hidden in the other representations of the dynamics.

III. QUANTITATIVE CHARACTERIZATION OF THE TRANSITION TO COHERENCE COLLAPSE

To understand the previous results in this section I investigate the behavior of the autocorrelation function of the complex electric field, the Lyapunov spectrum, the fractal dimension, and the metric entropy, when γ and τ vary.

The correlation function

$$G_E(t)=\frac{\langle E^*(t'+t)E(t')\rangle}{\langle E(t')^2\rangle} \tag{5}$$

expresses the correlations between the fields $E(t'+t)=E(t'+t)\exp[i\phi(t'+t)]$ and $E(t)=E(t)\exp[i\phi(t)]$ at two temporally separated points. [$|G_E(t)|$ is also the laser visibility, and in Ref. 18 the experimentally measured visibility curve of a laser diode operating in the coherence collapsed regime was accurately reproduced by the Lang and Kobayashi model; using parameters values approximately equal to those of Table I].

The autocorrelation function $G_E(t)$ is appropriate for the coherence collapsed regime because it is sensitive to variations in the phase of the electric field. Figure 6 shows $|G_E(t)|$ for $\gamma=3.5$ GHz and $\tau=10$ ns. $|G_E(t)|$ presents peaks at multiples of the relaxation oscillation period τ_R, and revival peaks at multiples of the delay time τ (the revival peaks were not considered in Ref. 18 because the visibility curves were measured for $t\ll\tau$). The revival peaks appear because $G_E(t)$ is related (by the Wiener-Khintchine theorem) to the Fourier transform of the optical spectrum, and the optical spectrum presents peaks at harmonics of the frequencies $f_{\text{rsol}}=1/\tau_R$ and $f_{\text{ext}}\approx 1/\tau$.

Therefore, the fields $E(t)$ and $E(t+\Delta t)$ are almost uncorrelated if Δt is small relative to τ, but strongly correlated if $\Delta t\approx\tau$. This explains the space-time features found in the 2D patterns. There is a slow decay of correlations (occurring on several delay units) that is responsible for the ''temporal'' disorder, and there is a fast decay (occurring on several relaxation oscillation periods) that is responsible for the ''spatial'' disorder.

Varying γ and τ I found that the decay of correlations is much faster when γ increases than when τ increases.

I used Farmer's method[12] to compute the Lyapunov spectrum, and calculated the metric entropy from the Pesin relation

$$h_\mu=\sum_{i=1}^{k}\lambda_i^+ \tag{6}$$

(where λ_i^+ are the positive Lyapunov exponents), and the fractal dimension from the Kaplan–Yorke formula

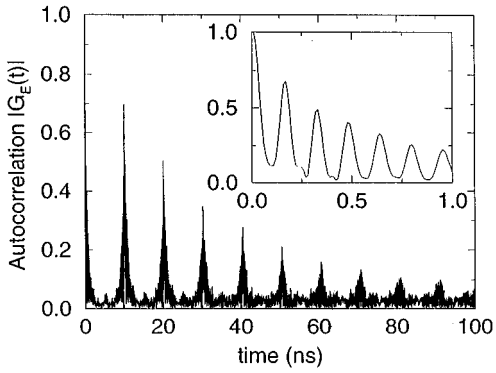

FIG. 6. Autocorrelation function of the complex electric field for $\tau=10$ ns and $\gamma=3.5$ GHz. $G_E(t)$ was calculated as the inverse Fourier transform of the optical spectrum: 65536 data points (sampled with $\Delta t=0.01$ ns) were used, which span 655 delay units. The inset shows the first few peaks of $|G_E(t)|$.

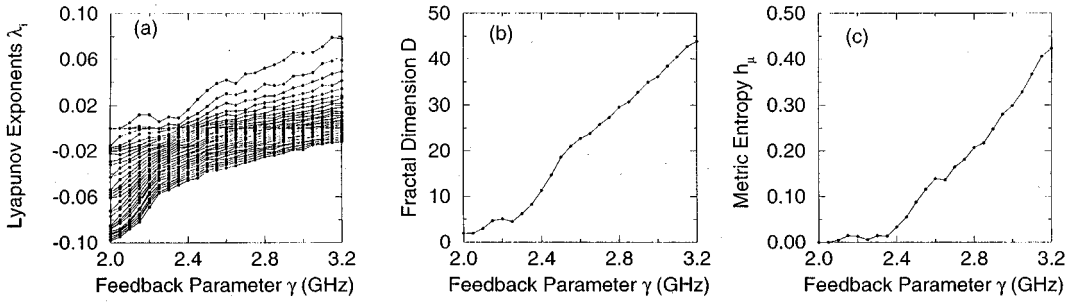

FIG. 7. Chaotic indicators for increasing γ and fixed τ ($\tau = 10$ ns). (a) Thirty largest Lyapunov exponents. Eighty Lyapunov exponents were computed. The integration time was 1000 delay units. (b) Fractal dimension, computed from Eq. (7). (c) Metric entropy, computed from Eq. (6).

$$D = j + \frac{\Sigma_{i=1}^{j} \lambda_i}{|\lambda_{j+1}|} \tag{7}$$

(where j is the largest integer for which $\Sigma_{i=1}^{j} \lambda_i \geqslant 0$).

Figure 7 shows the behavior of λ_i, D, and h_μ, when γ is increased while τ is kept constant. As γ increases there is a smooth transition to a high-dimensional chaotic state. All the Lyapunov exponents, both positive and negative, increase roughly linearly. D and h_μ also grows linearly with γ.

Figure 8 shows the behavior of λ_i, D, and h_μ, when the delay time is increased while the feedback level is kept fixed. The Lyapunov exponents remain finite or get smaller in absolute value as τ increases. D grows almost linearly with τ, and h_μ converges to a finite value. The entropy in this case is considerably smaller than when γ increases [compare the vertical scales of Figs. 7(c) and 8(c)]. As discussed in the Introduction, the behavior of λ_i, D, and h_μ with τ has been found in other time-delayed systems.

These results give increasing evidence of a transition to a ''weakly turbulent'' regime as τ increases, and to a ''highly turbulent'' regime as γ increases.

In the coherence collapsed regime, the total number of ECM attractor ruins in the global attractor increases with either γ or τ. Therefore, the volume of the global attractor grows with either γ or τ, and is natural to expect that the fractal dimension grows with either γ or τ. This is analogous to the behavior of an extended spatiotemporal chaotic system, for which the dimension of the attractor increases with the volume of the system. However, while τ only increases the number of degrees of freedom of the dynamics, γ also increases its disorder.

IV. SUMMARY AND CONCLUSIONS

I have done a detailed characterization of the transition to the coherence collapsed regime, in the case where an optical feedback is from a distant reflector. I used the 2D representation of delayed dynamical systems to rearrange the 1D time sequences of the output intensity and phase delay in the external cavity as 2D patterns. The quasiperiodic and chaotic patterns obtained allow the visualization of space-time-like features of the dynamics hidden in the long 1D series of data, and allow the recognition of two distinct types of transitions to coherence collapse.

When the laser operates in a single external cavity attractor, the intensity pattern and the phase delay pattern are quasiperiodic patterns that present a structure of straight lines over a background of thin rolls. Coherence collapse arises when several external cavity attractors merge. In the patterns the straight lines break and defects appear, and the thin rolls present dislocations and asymmetries. The phase delay pattern also presents a phase structure, because the laser switches among attractor ruins that have different mean phase delay.

When the feedback parameter is increased the number of defects grows and the quasiperiodic structure of the pattern is lost. The phase delay pattern has a large number of thin

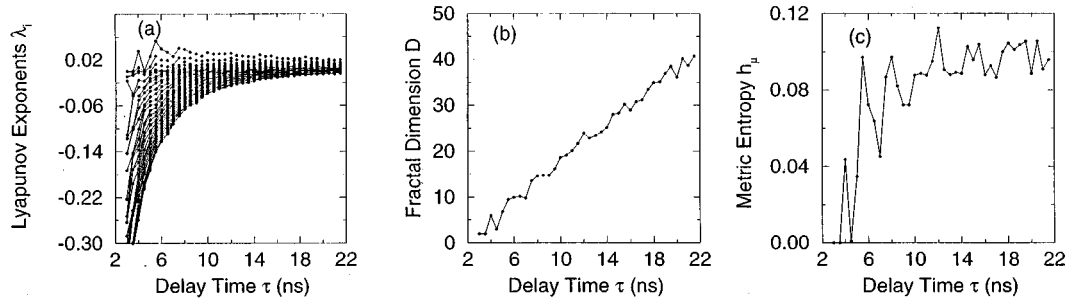

FIG. 8. Chaotic indicators for increasing τ and fixed γ ($\gamma = 2.5$ GHz). (a) Thirty largest Lyapunov exponents. (b) Fractal dimension. (c) Metric entropy.

phases, which reveals that a large number of attractors merge and that the jumps among them are frequent. In contrast, when the delay time is increased the number of defects in the patterns remains approximately constant, and there is a signature of the previous quasiperiodic structure (when the laser operated in a single attractor). Although the number of merged attractors increases, in the phase delay pattern there are phases of large width, which correspond to attractor ruins where the laser spends some time before switching to another.

These results suggest a transition to a developed turbulent regime when the feedback increases, and to a weakly turbulent regime when the delay time increases. This was confirmed by examining the behavior of various chaotic indicators. The autocorrelation function of the complex electric field decays much faster when γ increases than when τ increases. All the Lyapunov exponents (both positive and negative), the fractal dimension, and the metric entropy increase with γ. On the contrary, the Lyapunov exponents remain finite or decrease in absolute value with τ, the fractal dimension grows with τ, and the metric entropy converges to a finite value.

It would be interesting to study the correlations between the defects and the dislocations of the rolls, since it seems that the jumps among the attractor ruins have little or no role in the evolution of the rolls, but appear to be the origin of the apparition of defects. It would also be interesting to test the conjecture recently put forward by Egolf and Greenside[19] (in the context of extended systems), that the big fractal dimension of some large homogeneous chaotic systems might be accurately estimated by simple correlation functions calculations.

ACKNOWLEDGMENTS

I thank Professor N. Abraham for very useful discussions and Professor A. Albano for numerous comments on a preliminary version of this paper. This work was supported by the Project 47 of the BID-CONICYT, the Comision Sectorial de Investigacion Cientifica (CSIC) and the PEDECIBA. I also would like to thank Professor H. Chate for providing the computer software for the bidimensional patterns, and for his generous hospitality during my stay at CEA-Saclay.

[1] G. P. Agrawal and N. K. Dutta, *Long-Wavelength Semiconductor Lasers* (Van Nostrand, New York, 1986).
[2] Y. Kitaoka, H. Sato, K. Mizuuchi, K. Yamamoto, and M. Kato, IEEE J. Quantum Electron. **32**, 822–827 (1996).
[3] D. Lenstra, B. H. Verbeek, and A. J. Den Boef, IEEE J. Quantum Electron. **QE-21**, 674–679 (1985).
[4] J. Mork, B. Tromborg, and J. Mark, IEEE J. Quantum Electron. **28**, 93–107 (1992).
[5] R. Lang and K. Kobayashi, IEEE J. Quantum Electron. **QE 16**, 347–355 (1980).
[6] N. Schunk and K. Petermann, IEEE J. Quantum Electron. **24**, 1242–1247 (1988).
[7] J. Sacher, W. Elsässer, and E. O. Göbel, IEEE J. Quantum Electron. **27**, 373–379 (1991).
[8] H. Haug and H. Haken, Z. Phys. **204**, 262–275 (1967).
[9] C. H. Henry, IEEE J. Quantum Electron. **QE-18**, 259–264 (1982).
[10] C. Masoller, Phys. Rev. A **50**, 2569–2578 (1994).
[11] C. Masoller, Opt. Commun. **128**, 363–376 (1996).
[12] J. D. Farmer, Physica D **4**, 366–393 (1982).
[13] K. Ikeda and K. Matsumoto, J. Stat. Phys. **44**, 955 (1986); Physica D **29**, 223–235 (1987).
[14] M. Le Berre, E. Ressayre, A. Tallet, and H. M. Gibbs, Phys. Rev. Lett. **56**, 274 (1986).
[15] S. Lepri, G. Giacomelli, A. Politi, and F. T. Arecchi, Physica D **70**, 235–249 (1993).
[16] F. T. Arecchi, G. Giacomelli, A. Lapucci, and R. Meucci, Phys. Rev. A **45**, R4225–R4228 (1992).
[17] G. Giacomelli, R. Meucci, A. Politi, and F. T. Arecchi, Phys. Rev. Lett. **73**, 1099–1102 (1994).
[18] C. Masoller, C. Cabeza, and A. Sicardi Schifino, IEEE J. Quantum Electron. **31**, 1022–1028 (1995).
[19] D. A. Egolf and H. S. Greenside, Phys. Rev. Lett. **74**, 1751–1754 (1995).